Precipitating Snow Retrievals from Combined Airborne Cloud Radar and Millimeter-Wave Radiometer Observations

MIRCEA GRECU

Goddard Earth Sciences and Technology Center, University of Maryland, Baltimore County, Baltimore, and NASA Goddard Space Flight Center, Greenbelt, Maryland

WILLIAM S. OLSON

Joint Center for Earth Systems Technology, University of Maryland, Baltimore County, Baltimore, and NASA Goddard Space Flight Center, Greenbelt, Maryland

(Manuscript received 2 March 2007, in final form 4 October 2007)

ABSTRACT

An algorithm for retrieving snow over oceans from combined cloud radar and millimeter-wave radiometer observations is developed. The algorithm involves the use of physical models to simulate cloud radar and millimeter-wave radiometer observations from basic atmospheric variables such as hydrometeor content, temperature, and relative humidity profiles and is based on an optimal estimation technique to retrieve these variables from actual observations. A high-resolution simulation of a lake-effect snowstorm by a cloud-resolving model is used to test the algorithm. That is, synthetic observations are generated from the output of the cloud numerical model, and the retrieval algorithm is applied to the synthetic data. The algorithm performance is assessed by comparing the retrievals with the reference variables used in synthesizing the observations. The synthetic observation experiment indicates good performance of the retrieval algorithm. The algorithm is also applied to real observations from the Wakasa Bay field experiment that took place over the Sea of Japan in January and February 2003. The application of the retrieval algorithm to data from the field experiment yields snow estimates that are consistent with both the cloud radar and radiometer observations.

1. Introduction

Snow is an important component of the earth's hydrological cycle. Over land, in some regions and seasons, snow may be the only form of precipitation, and therefore it is very important for water resources management and planning. Also, over land, snow may be associated with severe weather that impacts human lives. Over land or oceans, snow is important because it influences the atmosphere's thermal structure through release of latent heating and radiative cooling. For these reasons, snow has been systematically studied from hydrologic, severe-weather, and climate standpoints.

The advent of spaceborne radars provides new opportunities for studying snow. Although spaceborne precipitation radars have difficulties detecting snow because of sensitivity limitations, spaceborne cloud radars operating at the W band are instruments that can provide unprecedented insight into various aspects of snow formation, global distribution, and interaction with other atmospheric or land processes. Such an instrument is the 94-GHz cloud-profiling radar (CPR) aboard the Cloud Satellite Mission (CloudSat). Although the CloudSat CPR itself can provide valuable information, it is expected that in conjunction with observations from other instruments (such as microwave radiometers) better interpretations of the CPR observations can be achieved.

Radar observations cannot be uniquely converted into snow contents because the size distribution of particles in the radar's observing volumes cannot be expressed as functions of single variables and usually at least two variables are necessary to describe the size distributions of snow particles. This makes the relationships of reflectivity versus snow content variable in time

Corresponding author address: Dr. Mircea Grecu, NASA Goddard Space Flight Center, Code 613.1, Greenbelt, MD 20771.
E-mail: grecu@agnes.gsfc.nasa.gov

DOI: 10.1175/2007JAMC1728.1

© 2008 American Meteorological Society

and space and the snow content estimates from radar-only observations subject to uncertainties. Coincident radiometer information can be used to reduce these uncertainties.

Precipitation estimates consistent with both radar and radiometer observations are preferable to radar-only estimates also because they facilitate the development of better radiometer-only algorithms. Methods to retrieve solid-phase hydrometeors from high-frequency radiometer-only observations have been developed by Evans et al. (2005), Seo and Liu (2005), and Noh et al. (2006). The existence of a realistic a priori database of hydrometeor profiles is crucial to the success of radiometer-only retrievals of solid-phase hydrometeors. This is clearly stated in the work of Evans et al. (2005), Seo and Liu (2005), and Noh et al. (2006). To construct a priori databases of hydrometeor profiles, these authors use radar-only observations. However, as has been demonstrated by Grecu and Olson (2006) for rain, it is possible to use combined radar–radiometer retrievals to construct a priori databases for radiometer-only retrievals of hydrometeors. Databases derived from combined radar–radiometer observations are potentially more compact and easier to explore than those derived from radar-only observations because the use of coincident radiometer observations limits the number of solutions that can be associated with a given reflectivity profile.

The objective of this paper is the development and the evaluation of an overocean algorithm for snow retrieval from coincident cloud radar and microwave millimeter-wavelength radiometer observations. The algorithm is developed and preliminarily tested using numerical simulations. That is, a cloud-resolving model (CRM) is used to simulate a specific snow process (lake-effect snow). Radar and radiometer observations are synthesized from the CRM output. The variables that significantly affect the synthesized radar and radiometer observations are identified, and a mathematically rigorous algorithm to retrieve them is formulated based upon the optimal estimation theory (Gelb 1974). The algorithm is applied to the synthesized observations, and its performance is assessed. The algorithm is also applied to actual observations from the Wakasa Bay experiment, which took place in Japan in January 2003, and the results are analyzed. Note that Skofronick-Jackson et al. (2003) developed a retrieval algorithm applicable to coincident radar and high-frequency radiometer observations. However, their algorithm is not based on the optimal estimation theory and may be less robust.

The paper is organized as follows: the next section describes the method used in the paper to determine the scattering properties of snowflakes. The numerical simulation of satellite cloud radar and radiometer observations is described in section 3. The retrieval algorithm formulation and its evaluation based on the numerical experiment are described in section 4. Section 5 contains results from the application of the algorithm to data from the Wakasa Bay experiment. Conclusions are provided in section 6.

2. Electromagnetic scattering properties of snowflakes

The relationships between the scattering properties of snowflakes (i.e., extinction and scattering efficiencies, and the asymmetry factor) and their sizes can be a major source of uncertainty in snow estimation from satellite observations. This is because snowflakes have highly complex and variable geometries (habits), and the solution of Maxwell's equations is difficult to determine for such particles. However, appropriate numerical techniques to solve Maxwell equations for complex ice geometries, although computationally expensive, exist. The discrete dipole approximation (DDA) of Draine and Flatau (1994) is such an approach. Using the DDA approach, Kim (2006) determined the scattering properties of ice crystals with different habits over a range of millimeter-wave frequencies and plotted them against the effective size parameter defined as

$$x_{\mathrm{eff}} = 2\pi r_{\mathrm{eff}}/\lambda, \tag{1}$$

where r_{eff} is the effective radius, that is, the radius of a sphere of pure ice with the same mass as that of the actual ice crystal. She concluded that the electromagnetic scattering properties do not significantly depend on the ice habit for size parameters that are smaller than 2.5. Here, using the same DDA approach of Draine and Flatau (1994), we analyze the scattering properties of ice crystals with two geometries: single cylinders and two orthogonal cylinders joined at their centers. The analysis suggests that a subtle dependency of scattering properties on the ice habit in fact exists. This finding is consistent with those of Weinman and Kim (2007) who postulated that the electromagnetic properties depend on the ice habit and also on the effective dimension Δ, defined as the ratio of the ice crystal volume to its average projected area.

To investigate further the dependence of scattering properties on the ice habit, we use an additional numerical tool to solve Maxwell's equations: the generalized multiparticle Mie (GMM) approach of Xu and Gustafson (2001). The GMM approach is based on addition theorems for vector spherical wave functions and allows a quasi-analytical solution of Maxwell's equation

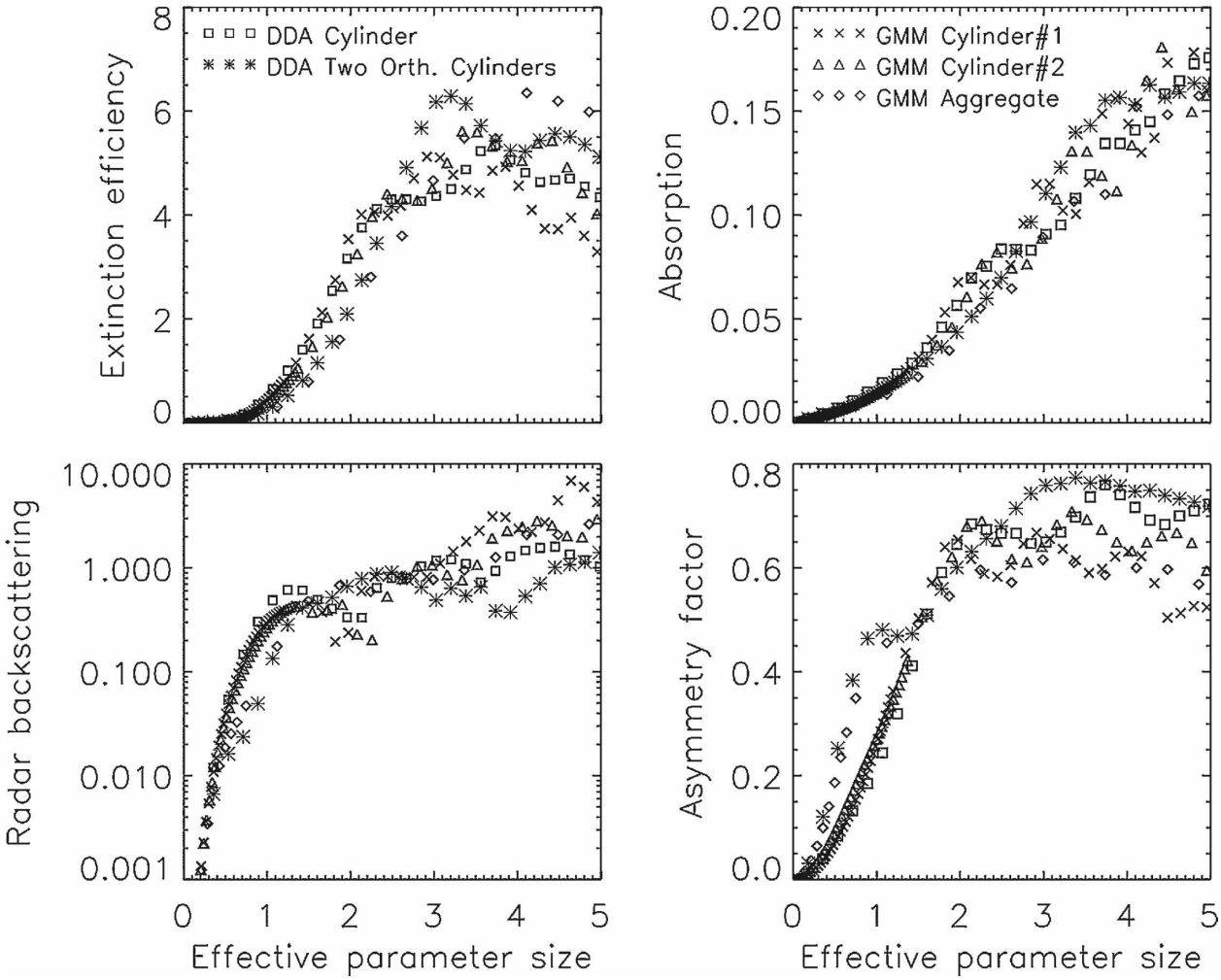

FIG. 1. Electromagnetic scattering properties determined using the GMM and the DDA approaches. The density is 0.125 g cm^{-3} for both the single-cylinder and the two-orthogonal-cylinder habit used in the DDA calculations. The densities of the GMM-approximated cylinders are 0.125 and 0.065 g cm^{-3}, respectively.

for multiple spheres. For a certain class of problems that involve the scattering from a relatively small number (e.g., 30) of spheres, the GMM approach is computationally more efficient than the DDA. Here, various types of ice particles are approximated by spheres and the GMM approach is applied. These types consist of single cylinders, two orthogonal cylinders joined at their centers, and aggregates. For cylinders, a relatively small number of spheres, not exceeding 30, are aligned along a single axis to approximate the single cylinder or along two orthogonal axes to approximate the two orthogonal, joined cylinders. For aggregates, although numerical simulations based on the coalescence equation can be used to generate snowflakes as clusters of osculating spheres (Maruyama and Fujiyoshi 2005), we use a simple statistical algorithm (Filippov et al. 2000) to generate ice crystals consisting of osculating spheres. Herein, because of computational considerations, we limit the number of spheres that form the aggregates to 30.

Representations of the scattering properties as a function of the effective size parameter from the DDA and the GMM approaches are shown in Fig. 1. Note that the scattering properties of single cylinders from both the DDA and GMM approaches do not significantly differ for size parameters of less than 2.5, irrespective of their densities. The effective density of the cylinder, defined as the mass divided by a spherical volume with a diameter equal to the maximum dimension of the cylinder, specified in the DDA calculations is 0.125 g cm^{-3}. The density of the two-cylinder habit used in the DDA calculations is also 0.125 g cm^{-3}. One of the approximated cylinders in the GMM approach has the same density (cylinder 1 in Fig. 1), and the other

(cylinder 2) is characterized by a density of 0.065 g cm^{-3}. It is apparent in Fig. 1 that the single-scattering properties of the two-orthogonal-cylinder habit determined from the DDA approach differ from those of the single cylinder also determined from the DDA approach. Moreover, the single-scattering properties of the multisphere aggregate determined from the GMM approach are similar to those of the two-orthogonal-cylinder habit and different from those of the single cylinder. Based on these calculations, we conclude that, although some of the scattering dependence on density may be parameterized through the use of the effective size parameter, there is also a dependence on the effective dimension (Weinman and Kim 2007) that is more difficult to parameterize. Because an exhaustive investigation of all types of possible particles is prohibitive from the computational standpoint, we will assume here that the properties of the two-orthogonal-cylinder habit are representative of the properties of snow particles in general. Therefore, given a certain snow particle with a known maximum diameter, its density is estimated using the Magono and Nakamura (1965) relationship (see section 3), and the effective size parameter is determined from the particle's mass. The scattering properties are then set based on the two-orthogonal-cylinder DDA calculations as a function of the effective size parameter.

In the future, we intend to use a more realistic aggregation model (e.g., Westbrook et al. 2004) to generate snow particles and then to calculate their scattering properties using the DDA approach. Given that aggregation models have been shown to reproduce realistically the properties of snow particles observed in nature [e.g., density–size relationships and particle size distribution; Westbrook et al. (2004)], the single-scattering properties derived from such an approach are potentially more realistic than those derived in the current study.

3. Simulation of a lake-effect snow

Here, the Advanced Regional Prediction System (ARPS; Xue et al. 2000) is used to simulate a lake-effect snowstorm. This kind of snowstorm is preferred to others because realistic results can be obtained with a relatively modest computational effort. The mechanism responsible for the production of lake-effect snow has been documented and numerically simulated in various studies (e.g., Cooper et al. 2000) and is only briefly described herein. The lake-effect snow is a consequence of a cold-air outbreak over a large body of relatively warm water (such as the Great Lakes of North America). The warm water provides the energy and moisture to produce an internal boundary layer and to initiate moist convection. As the cold air moves across the body of water, the boundary layer grows and the convection intensifies, yielding substantial snowfall over the downwind (lee) shore of the lake.

The ARPS model is set up for a 2D simulation as follows. The simulation domain is 30 km in the horizontal plane and 10 km in the vertical direction, and it is assumed that the domain is oriented along the direction of the prevailing wind. Using this limited horizontal domain, it is only possible to simulate the development of snow in a limited area over the lake surface near the lee shore, where the development of the convective boundary layer is greatest. The grid spacing utilized is 100 m in the horizontal plane and varies from 10 to 50 m in the vertical direction, with the finest grid spacing near the surface and becoming gradually coarser with altitude. In this simulation, the Goddard Cloud Ensemble (GCE) microphysical scheme (Tao and Simpson 1993) is used, and a 1.5-order turbulent kinetic energy closure is employed to account for turbulence. The surface sensible heat and moisture fluxes are determined as functions of the surface air and water temperatures using bulk formulas employing constant drag coefficients. A minimum speed of 2 m s^{-1} is specified in the surface flux bulk formulas to ensure that moisture and heat are transferred from the surface into the atmosphere despite the simple formulations of surface fluxes.

The model is initialized using a cold sounding observed in the vicinity of Lake Michigan in January 1998. The sounding is very similar in terms of moisture and temperature to the sounding recorded during the Lake-Effect Snow Study Storm Project (Kristovich 1993) at Green Bay, Wisconsin, at 1200 UTC 17 December 1983. The initial sounding, surface wind speed, and lake surface temperature are prescribed uniformly over the model domain, but the atmosphere is modified by surface fluxes as it would be if the domain followed the airflow over the lake in a Lagrangian sense. The model is run for 6 h of simulation time, which is a typical time for the flow of cold air to traverse Lake Michigan. Although the simulation is 2D, the basic model setup and initialization roughly follow the investigation by Cooper et al. (2000). However, our purpose here is not to perform a case-study simulation of a particular lake-effect snow event, but rather to produce physically plausible lake-effect convective snow and hydrometeor distributions for the purpose of testing a snow remote sensing algorithm.

The GCE microphysical scheme features seven species of water. Of these, only four—water vapor, cloud liquid water, cloud ice, and snow—attain nonzero val-

ues in this simulation. The GCE microphysical scheme is based on the assumption that precipitation (snow) particle size distributions (PSDs) can be described by exponential laws with fixed intercepts. This assumption is not appropriate for studying the benefit of incorporating information from radiometer observations in a radar retrieval algorithm, because both radar reflectivities and microwave radiances are sensitive to higher moments of the PSDs. Therefore, in this study, it is assumed that the snow PSDs can be properly described as normalization gamma functions (Testud et al. 2001):

$$N(D) = N_0^* f(\mu)\left(\frac{D}{D_0}\right)^{\mu} \exp[-(3.67 + \mu)D/D_0], \quad \text{with} \tag{2}$$

$$f(\mu) = \frac{6}{3.67^4}\frac{(3.67 + \mu)^{(4+\mu)}}{\Gamma(3.67 + \mu)}, \tag{3}$$

where N_0^* is a generalized intercept, μ is a shape parameter, D is the particle diameter, and D_0 is median diameter. Testud et al. (2001) found that relationships between the electromagnetic properties of hydrometeors integrated over their size distributions and the hydrometer content depend mainly on N_0^* and only weakly on μ. The generalized intercept N_0^* varies horizontally as well as vertically. However, its altitude dependence can be parameterized as shown by Heymsfield et al. (2002) and Field and Heymsfield (2003). Thus, the intercept at altitude z, $N_0^*(z)$, can be expressed as a function of scaling intercept at altitude z_0 as

$$N_0^*(z) = N_0^*(z_0) \exp\{-0.374[T(z) - T(z_0)]\}, \tag{4}$$

where $T(z)$ is the temperature at height z. Relationship (4), although formulated in terms of temperatures, expresses the dependence of N_0^* on altitude and microphysical processes in the vertical direction.

To complete the information needed to simulate brightness temperatures and radar reflectivities rigorously, intercepts $N_0^*(z_0 = 0, x)$ are generated at random for each bottom boundary grid cell in the computational domain. The intercepts are generated from a lognormal distribution with parameters similar to those in Testud et al. (2001). Then, using (4), vertical profiles of scaling parameter $N_0^*(z, x)$ are determined as a function of $N_0^*(z_0 = 0, x)$. Note that although the surface intercepts are generated randomly from grid cell to grid cell in the horizontal plane, any spatial correlations of simulated snow water contents in the horizontal plane lead to correlations of median particle sizes in the horizontal plane as well. The snow particle ice/air density is determined as a function of particle maximum diameter using the following parameterization (Magono and Nakamura 1965):

$$\rho = 0.07D^{-1}, \tag{5}$$

where ρ (g cm^{-3}) is the density and D (cm) is the maximum diameter of the snow particle.

The electromagnetic scattering properties of snow are determined based on the DDA calculations described in the previous section as a function of the snow content. The shape parameter μ is arbitrarily set to 0 everywhere in the computational domain, given that its value affects only weakly the relationships between the electromagnetic scattering properties and the snow contents. The scattering properties of cloud ice are determined based on the relationships of Heymsfield and Platt (1984), as described by Olson et al. (2001). The cloud water and water vapor extinction efficiencies are determined as described in Grecu and Anagnostou (2002), and the brightness temperatures at various millimeter-wave frequencies are calculated using an Eddington approximation (Grecu and Anagnostou 2002) for an angle of incidence of 0.0°. For the surface emissivity, we use the model implemented in the Goddard Profiling Algorithm (Kummerow et al. 2001). The radiometer frequencies consist of 89, 150, 183.3 ± 1, 183.3 ± 3, 183.3 ± 7, and 220 GHz, which are the frequencies of the millimeter-wave imaging radiometer (MIR), deployed in various field campaigns.

Shown in Fig. 2 are the simulated brightness temperatures and the simulated attenuated radar reflectivities at 94 GHz (W band). Note in Fig. 2 that the 89-GHz radiances exhibit both emission (positive excursions) and scattering (negative excursions), relative to a background brightness temperature of approximately 205 K, although preponderantly emission is seen. The 150-GHz radiances exhibit mainly scattering (negative excursions relative to a background of about 230 K), although some emission signatures are still evident. Two of the water vapor absorption channels, that is, 183.3 ± 3 and 183.3 ± 7, exhibit scattering signatures, and the 183.3 ± 1 GHz brightness temperatures are essentially constant. The 183.3 ± 1 GHz is mostly sensitive to the relative humidity in the atmospheric layer extending from 5.0 to 12.0 km, an atmospheric layer that does not exhibit notable variation in the numerical model. Therefore, the 183.3 ± 1 GHz brightness temperatures are invariant in this simulation. The 220-GHz brightness temperatures are similar to those at 183.3 ± 7 GHz and are strongly correlated with the path-integrated attenuation (PIA). The PIA is the total attenuation of a radar pulse as it passes down through the atmosphere, is reflected off the earth's surface, and passes upward

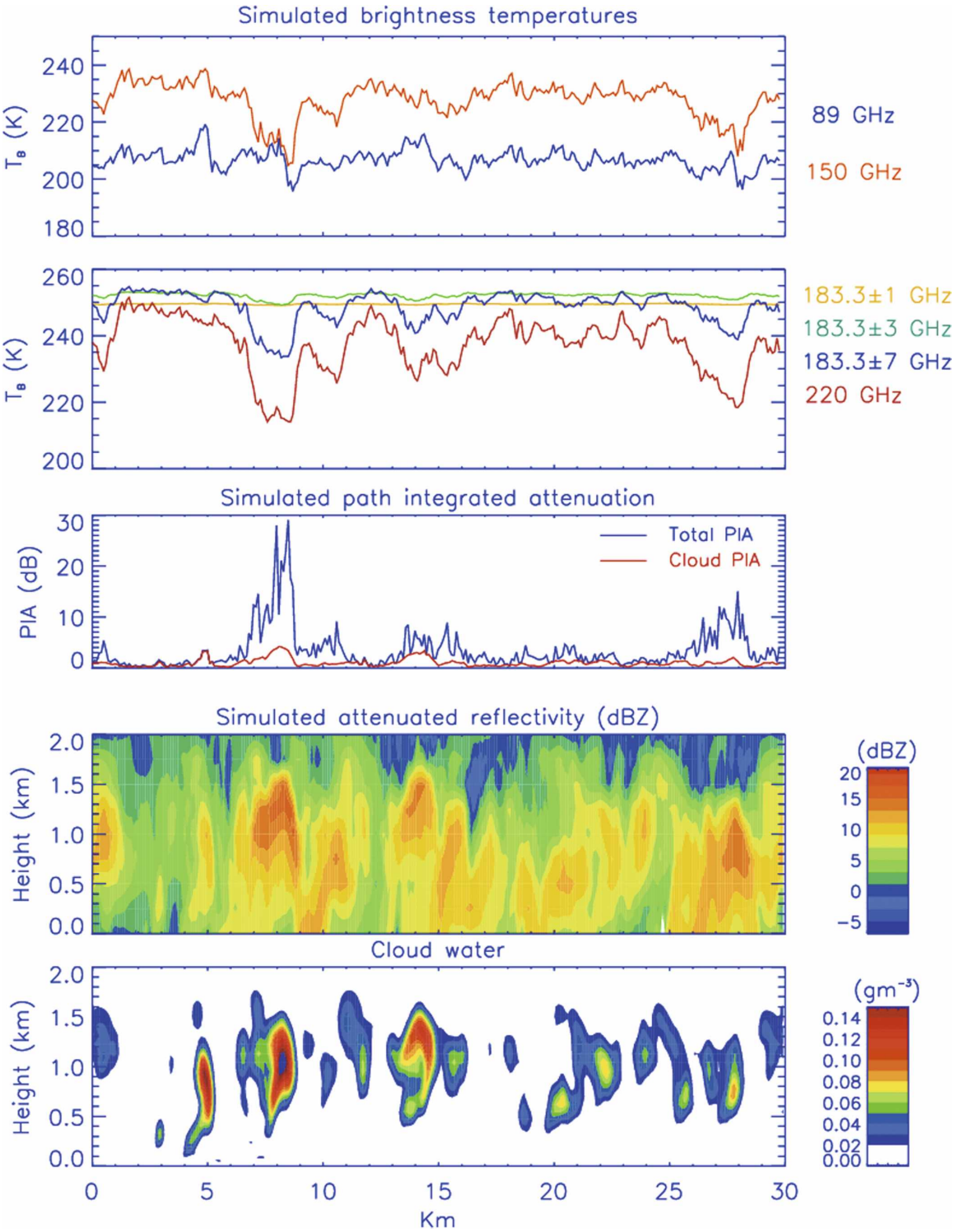

FIG. 2. Brightness temperatures, PIA, radar reflectivities, and cloud liquid water contents derived from a cloud-model simulation of lake-effect snow.

through the atmosphere again to the receiver. The total PIA due to all atmospheric constituents, as well as the PIA contribution from cloud liquid water alone, is shown in the figure. Also shown in Fig. 2, in the bottom panel, are the simulated cloud liquid water contents. Although the simulated cloud liquid water contents are somewhat dependent on the particular microphysical scheme used in this study, cloud water is nonetheless an important constituent that participates in ice microphysical processes (Lin et al. 1983). Radiometer observations from field campaigns (as apparent in section 5) suggest nonnegligible quantities of liquid water in precipitating snow clouds. As seen in Fig. 2, cloud liquid water accounts on average for 30% of the total PIA in the simulated snow clouds. Therefore, cloud liquid water should be taken into account explicitly in algorithm development, because it affects both the radar observations through attenuation and the 89.0-GHz brightness temperatures through emission, in particular, which makes the synthetic data in Fig. 2 suitable for testing combined radar–radiometer snow retrieval algorithms.

4. Retrieval method: Formulation and application to synthetic observations

As apparent from Fig. 2, attenuation of the observed reflectivity may be severe, which makes the retrieval difficult. This is because the attenuation correction using the analytical approach of Hitschfeld and Bordan (1954) may be unstable when the attenuation is large (Iguchi and Meneghini 1994). Moreover, the presence of cloud liquid water, which is responsible for some of the attenuation of the observed reflectivities, can make it impossible to express the attenuation as a function of reflectivity alone, in the way it is assumed in the Hitschfeld–Bordan approach. The Hitschfeld–Bordan approach requires that the attenuation k be related to reflectivity Z through a power-law relationship of the type $k = \alpha Z^{\beta}$. The parameter β has to be constant with range for the analytical solution to be valid. However, because the fraction of cloud liquid water varies in time and space (and possibly independent of Z), β is not constant with range. Therefore, in this study, in a departure from previous work on the development of a combined precipitation retrieval algorithm by Grecu and Anagnostou (2002), the Hitshfeld–Bordan solution is not used at all. Instead, a set of unknown variables $\mathbf{X}$ consisting of the PSD intercept at the surface $N_0^*(z_0 = 0)$, a cloud-scaling parameter x_c, snow equivalent water contents at the levels at which radar observations are available $\mathbf{w}_s$, and three relative humidity principal components **RHPC** is defined. In our formulation, cloud ice is not explicitly retrieved. Instead part of the snow is assumed to be cloud ice. The cloud water profile is determined by multiplying a generic cloud water profile (the average of all cloud water profiles in the computational domain) by x_c. The PSD intercepts at heights different from zero are determined using (4). The relative humidity profile is determined from the **RHPC** using

$$\mathbf{RH}(z) = \sum_{i=1}^{3} \mathrm{RHPC}_i \times \mathbf{RHEOF}_i(z), \tag{6}$$

where $\mathbf{RHEOF}_i$ are the first three empirical orthogonal functions (EOFs) of the relative humidity. Equation (6) provides a reduction in the number of variables needed to represent the vertical variation in relative humidity. Because the relative humidity is an autocorrelated variable (i.e., its value at a certain location in space is partially correlated with its values at other locations in space), a transform exists (North 1984) that makes it possible to approximate relative humidity profiles as a combination of a small number of profiles called empirical orthogonal functions (EOFs). The advantage of using relative humidity EOFs resides in the fact that only a few of them need to be considered to approximately reconstruct any relative humidity profile. In our simulation, the first three principal components explain more than 90% of the variability of all relative humidity profiles. In addition to using principal components to describe relative humidity profiles, to make the retrieval problem well posed we limit the principal component variability to within 10% of the values obtained in clear-air retrievals. The temperature profiles are assumed to be known and are set equal to their averages over the computational domain. The snow density is determined based on (5). (The sensitivity of the retrievals to the density assumption is examined below.) Thus, the attenuated radar reflectivities, PIAs, and the radiometer brightness temperatures can be determined as functions of

$$\mathbf{X} = \{N_0^*, x_c, \mathbf{w}_s, \mathbf{RHPC}\}.$$

The retrieval problem is equivalent to minimizing the following objective function:

$$\begin{aligned} F = {} & \frac{1}{2}[\mathbf{Z}^M - \mathbf{Z}(\mathbf{X})]^{\mathrm{T}}\mathbf{W}_Z^{-1}[\mathbf{Z}^M - \mathbf{Z}(\mathbf{X})] \\ & + \frac{1}{2}[\mathrm{PIA}_S - \mathrm{PIA}(\mathbf{X})]^{\mathrm{T}}\mathbf{W}_{\mathrm{PIA}}^{-1}[\mathrm{PIA}_S - \mathrm{PIA}(\mathbf{X})] \\ & + \frac{1}{2}[\mathbf{T}_B^M - \mathbf{T}_B(\mathbf{X})]^{\mathrm{T}}\mathbf{W}_T^{-1}[\mathbf{T}_B^M - \mathbf{T}_B(\mathbf{X})] \\ & + \frac{1}{2}(\mathbf{X}_N - \mathbf{X})^{\mathrm{T}}\mathbf{W}_N^{-1}(\mathbf{X}_N - \mathbf{X}), \end{aligned} \tag{7}$$

where $\mathbf{Z}^M$ and $\mathbf{Z}(\mathbf{X})$ are the observed and calculated reflectivities, $\mathbf{T}_B^M$ and $\mathbf{T}_B(\mathbf{X})$ are the observed and calculated brightness temperatures, and PIA($\mathbf{X}$) are the calculated path-integrated attenuations. In practice, the PIA_S are PIA estimates that can be derived from the surface reference technique (Meneghini et al. 2000), but here they are derived directly from the simulated attenuation. The vector $\mathbf{X}_N$ represents an a priori estimate of $\mathbf{X}$, here assumed to be the average of the unknowns over the model domain. The average values of $\{x_c, \mathbf{w}_s, \mathbf{RHPC}\}$ are determined using the CRM simulation, and the average of N_0^* is set based on the study by Testud et al. (2001). Likewise, the error covariance of the a priori estimate $\mathbf{W}_N$ is set based on the CRM simulation and the findings by Testud et al. (2001). Variables $\mathbf{W}_Z$, $\mathbf{W}_T$, and $\mathbf{W}_{\mathrm{PIA}}$ are assumed to be diagonal matrices. The diagonal elements of $\mathbf{W}_Z$ are set to 1.0 $\mathrm{dB}Z^2$, which corresponds to a typical radar reflectivity error of 1.0 dB. The $\mathbf{W}_T$ diagonal elements are set to 1.0 K^2, and a typical value for $\mathbf{W}_{\mathrm{PIA}}$ is 1.0 dB^2 according to Meneghini et al. (2000).

To minimize (7), the ideal Newton iterative method (Gill et al. 1981) is used. To estimate the tangent linear approximation of the observation operator, the ensemble-based method of Evensen (2006) is employed. That is, a number N of random solutions $\mathbf{X}_i$, where $1 \leq i \leq N$, are generated. Let the vector $\mathbf{Y}$ represent the set of observations $\mathbf{Z}$, PIA_S, and $\mathbf{T}_B$, and $\mathbf{H}(\mathbf{X}_i)$ represent the calculated observations. Based on $\mathbf{Y}$ and $\mathbf{H}(\mathbf{X}_i)$, each solution $\mathbf{X}_i$ of the ensemble is updated using the following formula:

$$\mathbf{X}_i' = \mathbf{X}_i + \mathbf{PH}^{\mathrm{T}}(\mathbf{HPH}^{\mathrm{T}} + \mathbf{R})^{-1}[\mathbf{Y} - \mathbf{H}(\mathbf{X}_i)], \quad (8)$$

where

$$\mathbf{PH}^{\mathrm{T}} = \frac{1}{N-1}\sum_{i=1}^{N}(\mathbf{X}_i - \overline{\mathbf{X}})[\mathbf{H}(\mathbf{X}_i) - \overline{\mathbf{H}(\mathbf{X})}]^{\mathrm{T}}, \quad (9)$$

$$\mathbf{HPH}^{\mathrm{T}} = \frac{1}{N-1}\sum_{i=1}^{N}[\mathbf{H}(\mathbf{X}_i) - \overline{\mathbf{H}(\mathbf{X})}][\mathbf{H}(\mathbf{X}_i) - \overline{\mathbf{H}(\mathbf{X})}]^{\mathrm{T}}, \quad \text{and} \quad (10)$$

$$\mathbf{R} = \begin{bmatrix} \mathbf{W}_Z & \mathbf{0} & \mathbf{0} \\ \mathbf{0} & \mathbf{W}_{\mathrm{PIA}} & \mathbf{0} \\ \mathbf{0} & \mathbf{0} & \mathbf{W}_T \end{bmatrix}. \quad (11)$$

The correct specification of $\mathbf{R}$ requires extensive CRM and radiative transfer modeling and/or in situ observations. Given the limited amount of CRM and in situ data available for this study, we chose to set $\mathbf{R}$ to a diagonal matrix as explained above. This is a simplification that might induce uncertainties in the retrievals but is a good alternative to estimating the full structure of $\mathbf{R}$ based on insufficient data (Marzano et al. 1999).

After the update, the error covariances (9) and (10) are recalculated and (8) may be applied again until convergence is achieved. The convergence criterion requires that no significant change in the average value of F (i.e., less than 5%) is obtained by a new iteration (where the average is determined by evaluating F for all the members of the ensemble). Equation (8) represents a second-order approach and is derived from the condition that the gradient of the objective function is zero, that is, $\nabla F = 0$, where F is the objective function (7). Convergence is typically achieved in four iterations for $N = 30$. The final estimate is given by the mean of the ensemble:

$$\overline{\mathbf{X}} = \frac{1}{N}\sum_{i=1}^{N}\mathbf{X}_i, \quad (12)$$

and an estimate of its uncertainty is

$$\mathbf{s}_X = \left[\frac{1}{N-1}\sum_{i=1}^{N}(\mathbf{X}_i - \overline{\mathbf{X}})(\mathbf{X}_i - \overline{\mathbf{X}})^{\mathrm{T}}\right]^{1/2}. \quad (13)$$

In applying the ensemble-based retrieval method to the synthetic radar–radiometer data, the 94-GHz radar reflectivities and PIAs as well as the 89-, 183 ± 1, and 183 ± 7 GHz brightness temperatures are utilized. Several variables retrieved from these synthetic observations are shown in Fig. 3. These include the liquid water path, the relative PSD intercept (defined as the ratio of the actual intercept N_0^* to a nominal value of 0.08 cm^{-4}, the Marshall–Palmer value), the snow water content, and the path-integrated attenuation. Good agreement between the retrieved variables and the actual variables derived from the model simulations is achieved. The relative PSD intercept exhibits the largest errors. However, because the reflectivity snow water content relationships depend on a subunitary power (with an exponent smaller than 0.5) of the relative PSD intercept (Testud et al. 2001; Grecu and Anagnostou 2002), the errors in the snow estimates are relatively smaller than those in the PSD intercepts. The cloud liquid water path also exhibits larger errors than the snow water content, most likely because the cloud water-sensitive 89-GHz brightness temperatures depend also on the surface wind speed, through its effect on water surface emissivity. The surface wind speed cannot be reliably retrieved from millimeter-wave observations and was not treated as an unknown in the formulation of (7). However, as is apparent from Fig. 3, this does not significantly impact the retrieval of the other variables.

Shown in Fig. 4 are the actual snow and retrieved snow contents. As described above, cloud ice is not

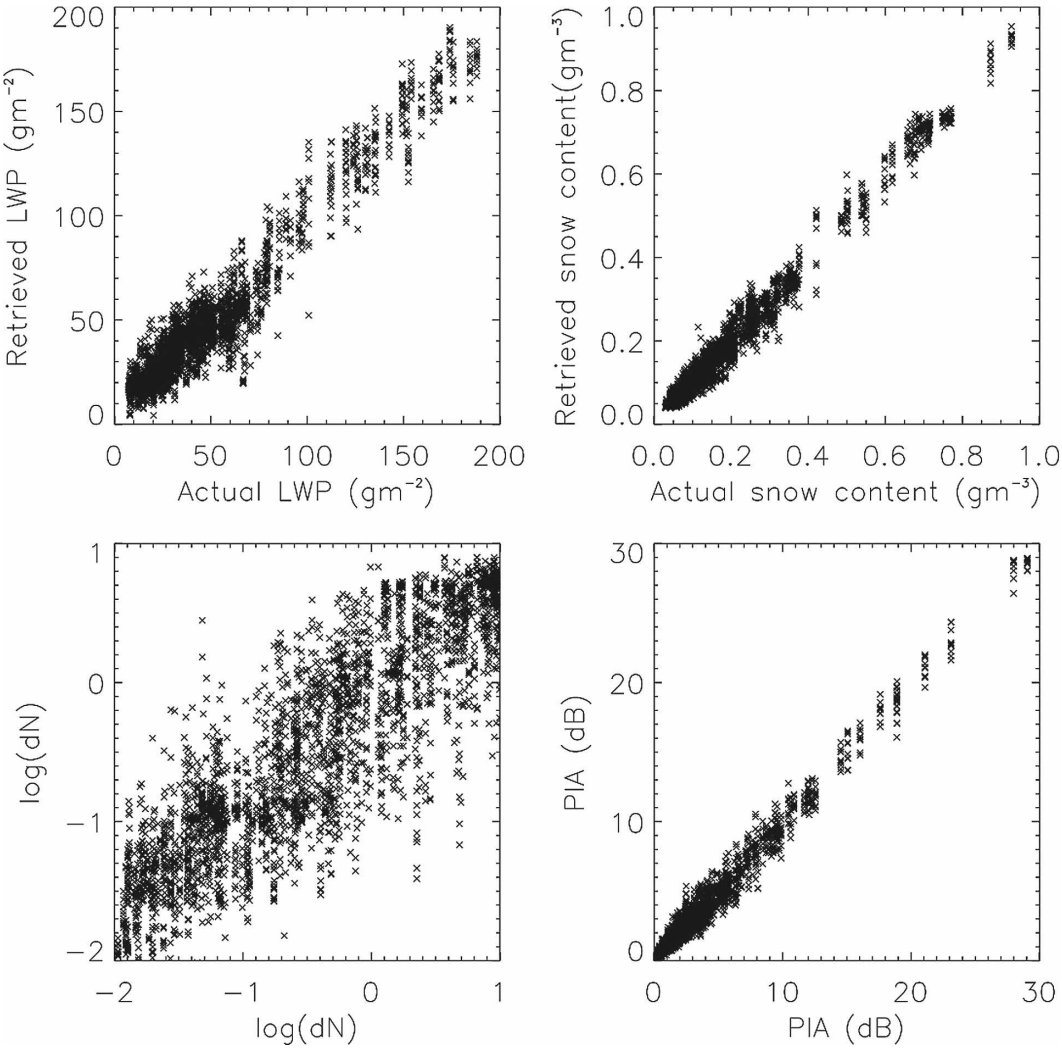

FIG. 3. Retrieved variables estimated from model-generated synthetic data, plotted against actual variables from the model simulation.

explicitly retrieved but is assumed to be part of the retrieved snow. To make the comparison consistent, the cloud ice and snow are combined into a category generically called snow in Fig. 4. It may be noticed in the figure that, consistent with results presented in Fig. 3, the actual and the retrieved values are highly correlated. Also shown in Fig. 4 are the differences between the retrieval using the correct snow density parameterization and a retrieval in which the equivalent densities are 2 times those estimated from (5). It is found that the retrieved variables, although still highly correlated with the actual variables, exhibit a bias of about −15%. This is because, as is apparent from Fig. 1, the radar backscattering as well the extinction and asymmetry factor for small particles increases with the density. This implies that the calculated radar reflectivities, the PIAs, and the scattering in the radiometer high-frequency brightness temperatures are overpredicted when assuming a snow density of 2 times the actual snow density. As a consequence, the minimization technique compensates by reducing the amount of snow in the retrieval to produce a better agreement between the actual observations and their optimized values. Because the estimation of snow density directly from radar and radiometer observations seems unfeasible, the best strategy to minimize the errors caused by uncertainties in snow density is to parameterize its values based upon independent observations such as airborne microphysical data.

In the next section the retrieval algorithm is applied to remote sensing observations from the Wakasa Bay experiment.

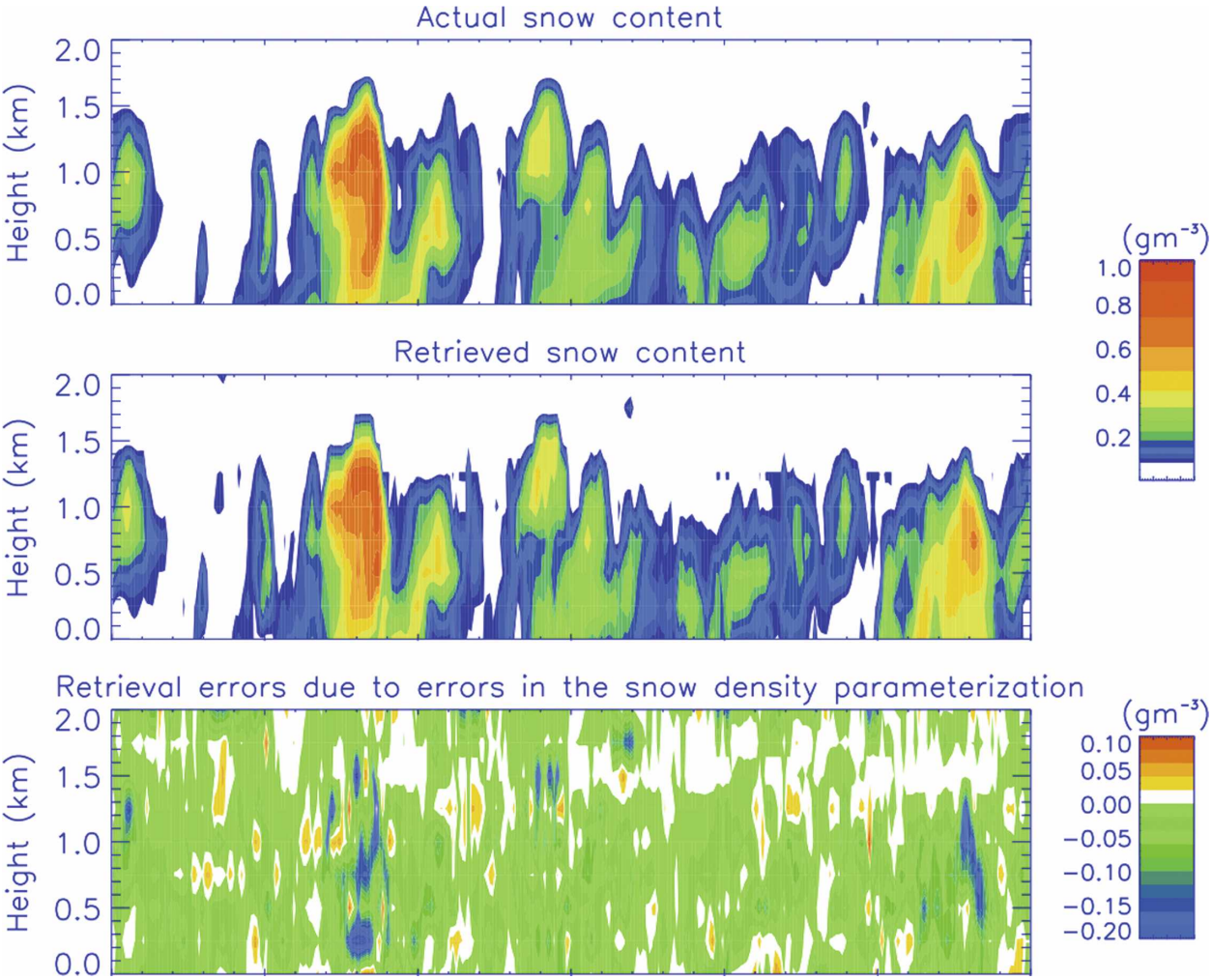

FIG. 4. Actual and retrieved snow contents and retrieval errors due to errors in the snow density parameterization.

5. Application to airborne data

The Wakasa Bay field experiment took place over the Sea of Japan from 3 January to 14 February 2003 (Lobl et al. 2007). The primary objective was to provide data for the validation of shallow rain and snow retrievals from the Advanced Microwave Scanning Radiometer—Earth Observing System (AMSR-E) observations. To achieve this objective, several instruments were deployed in the experiment. These include a dual-frequency precipitation radar (PR-2), an airborne cloud radar (ACR), an airborne multichannel microwave radiometer, and a MIR. Two of these instruments, that is, the ACR and the MIR, provide radar and radiometer observations that are useful for testing the retrieval algorithm presented in the previous section. Although many combinations of instruments and channels can be used to estimate precipitating snow, the ACR data are of particular interest because it operates at the same frequency as the CloudSat radar (94 GHz).

Shown in Fig. 5 are millimeter-wave brightness temperatures and ACR reflectivities collected during a flight leg on 19 January 2003. Note that the airborne observations in Fig. 5 are similar in many respects to the synthetic observations presented in section 2. For example, the 89- and 150-GHz data exhibit significant emission (e.g., the peak near 37.25°N latitude), which can be used to estimate the amount of liquid water in clouds but cannot be used to provide additional information on the precipitating snow. On the other hand, the brightness temperatures at the higher frequencies, such as 183.3 ± 3, 183.3 ± 7, and 220 GHz, exhibit scattering signatures and can provide additional information on the precipitating snow. Some differences with respect to the model simulations are obvious as well, the most obvious being that the observed precipi-

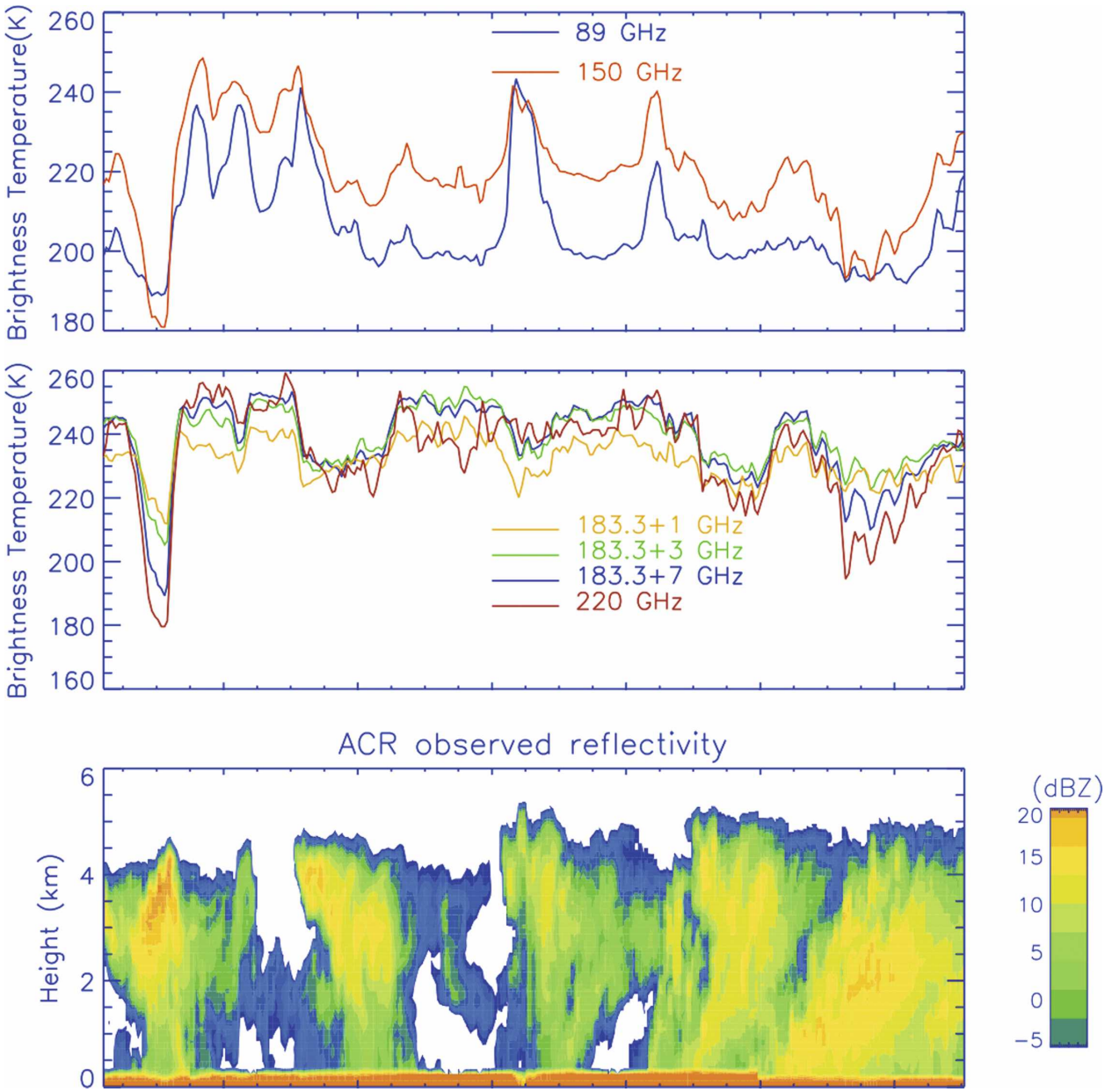

FIG. 5. MIR brightness temperatures and ACR reflectivities observed on 29 Jan 2003.

tating snow clouds are deeper than the simulated clouds. This difference is the outcome of frontal dynamics that were active during the Wakasa Bay observing period, whereas the simulated snow clouds are primarily controlled by boundary layer processes. Nevertheless, the overall similarity between the simulated and airborne observations is remarkable, and this result implies that the retrieval algorithm developed and tested using the synthetic data can be applied to actual data as well.

The retrieval algorithm is applied to the observations shown in Fig. 5. The snow densities are determined using the parameterization given by (5). The temperature profiles and the relative humidity EOFs are determined from National Centers for Environmental Prediction–National Center for Atmospheric Research reanalysis data (obtained online at ftp://ftp.cdc.noaa.gov/). That is, reanalysis data from the Wakasa Bay area on 19 January 2003 are used to determine an average temperature profile and the relative humidity EOFs. As in the retrievals based upon the synthetic data, only the 89-, 183.3 ± 1, and 183.3 ± 7 GHz bright-

ness temperatures are utilized in the estimation method, along with the radar observations and the PIA estimates from the surface reference technique (Meneghini et al. 2000). The 150-, 183.3 ± 3, and 220-GHz radiometer observations are used for validation. In other words, the brightness temperatures at these frequencies are calculated based upon the final retrieved variables, but the differences between the calculations and observations are not used in the estimation procedure itself. Instead, they are analyzed for the retrieval assessment.

The calculated and observed brightness temperatures at 89, 150, 183.3 ± 1, 183.3 ± 3, 183.3 ± 7, and 220 GHz are shown in Fig. 6, and one may note generally good agreement between these two sets of brightness temperatures. Even the calculated brightness temperatures at frequencies not used in the retrieval, that is, 150, 183.3 ± 3, and 220 GHz, agree well with the observed brightness temperatures. Greater discrepancies between the calculated and observed brightness temperatures are apparent in the region extending from approximately 37.7° to 37.9°N, for which the 183.3 ± 1 GHz calculated brightness temperatures are generally higher than the observed and the 183.3 ± 7 GHz brightness temperatures are generally lower than the observations. Simple changes in the estimated snow water contents cannot remove these discrepancies—uncertainties in the evaluation of the water vapor extinction, or uncertainties in the snow density relationship (5), could account for the biases in the calculated brightness temperatures.

Shown in Fig. 7 are the snow water content, the relative PSD intercept, the cloud liquid water path (LWP), and the PIA retrieved using the combined algorithm. As expected, the retrieved snow content patterns are well correlated with the radar reflectivity patterns. The relative PSD intercept is usually smaller than 1.0 and larger than 0.01. Lower values of the relative PSD intercept appear to be associated in some regions with large LWP values. Whether this is an artifact of the solution or is a consequence of ice microphysical processes remains to be investigated using CRMs employing explicit microphysics or through intensive field campaign studies in which in situ microphysical data are obtained. It is also apparent from Fig. 7 that the LWP may be very large and contribute significantly to the PIA. On the other hand, the retrieved LWP is not simply proportional to the total PIA. In other words, both snow and cloud liquid water contribute to the total PIA, and the combined radar and radiometer data provide enough information to distinguish their relative effects on PIA.

From both Figs. 5 and 7, it may be noted that the ACR reflectivities may be subject to severe attenuation. In the retrieval algorithm, radiometer brightness temperatures and a surface return–based estimate of the PIA are used to correct for the attenuation. Nevertheless, the attenuation correction is associated with errors. To evaluate how these errors affect the retrieval, the retrieval algorithm is applied to combined Ku-band radar channel of the PR-2 and MIR observations. The Ku-band radar observations of snow do not exhibit significant attenuation and consequently can be used to investigate the effect of attenuation in the cloud radar observations on the combined retrievals. The Ku-band PIA is negligible, and no reliable PIA estimate can be obtained from the surface return. Therefore, surface-return estimates of Ku-band PIA are not used in the retrievals. This is achieved computationally by setting $\mathbf{W}_{\mathrm{PIA}}$ to a large value (on the order of tens of squared decibels). All other covariance matrices and assumptions are the same as in the previous applications of the combined cloud radar–radiometer algorithm. The retrieved snow from the combined Ku-radar and MIR observations is shown in Fig. 8. Also shown in Fig. 8 are the differences between the combined W-band–MIR retrievals and the combined Ku-band–MIR retrievals. Note that the combined W-band–MIR retrievals are usually larger than the Ku-band–MIR retrievals above 2.0 km and are smaller below. The low-level W-band–MIR underestimation (relative to the Ku-band–MIR estimates) in some regions (around 36.7° and 37.2°N) is most likely caused by insufficient attenuation correction of the W-band observations. In these regions, the retrieval technique appears to underestimate the W-band effective (attenuation corrected) reflectivities and/or the PSD intercept. In other regions (e.g., from 37.6° to 37.9°N), the differences may be caused by lower sensitivity of the Ku-band radar to small particles at the top of the cloud. The main mechanism that the retrieval procedure uses to reconcile radar and radiometer observations is the adjustment of the PSD intercept. Through this mechanism, the insensitivity of Ku-band observations to small ice particles can be compensated through an increase in the PSD intercept. However, the PSD intercept is parameterized, and this may lead to an overestimation in regions of relatively high reflectivities where the Ku-band radar low sensitivity to small particles in not very important. As a consequence, the Ku-band overestimate at low levels may be not only an effect of the attenuation in the W-band observations but also a consequence of the reduced sensitivity of the Ku-band radar reflectivities to small ice particles. A rigorous quantification of the contributions of these two potential sources of errors as well as of other errors such those in the estimation of

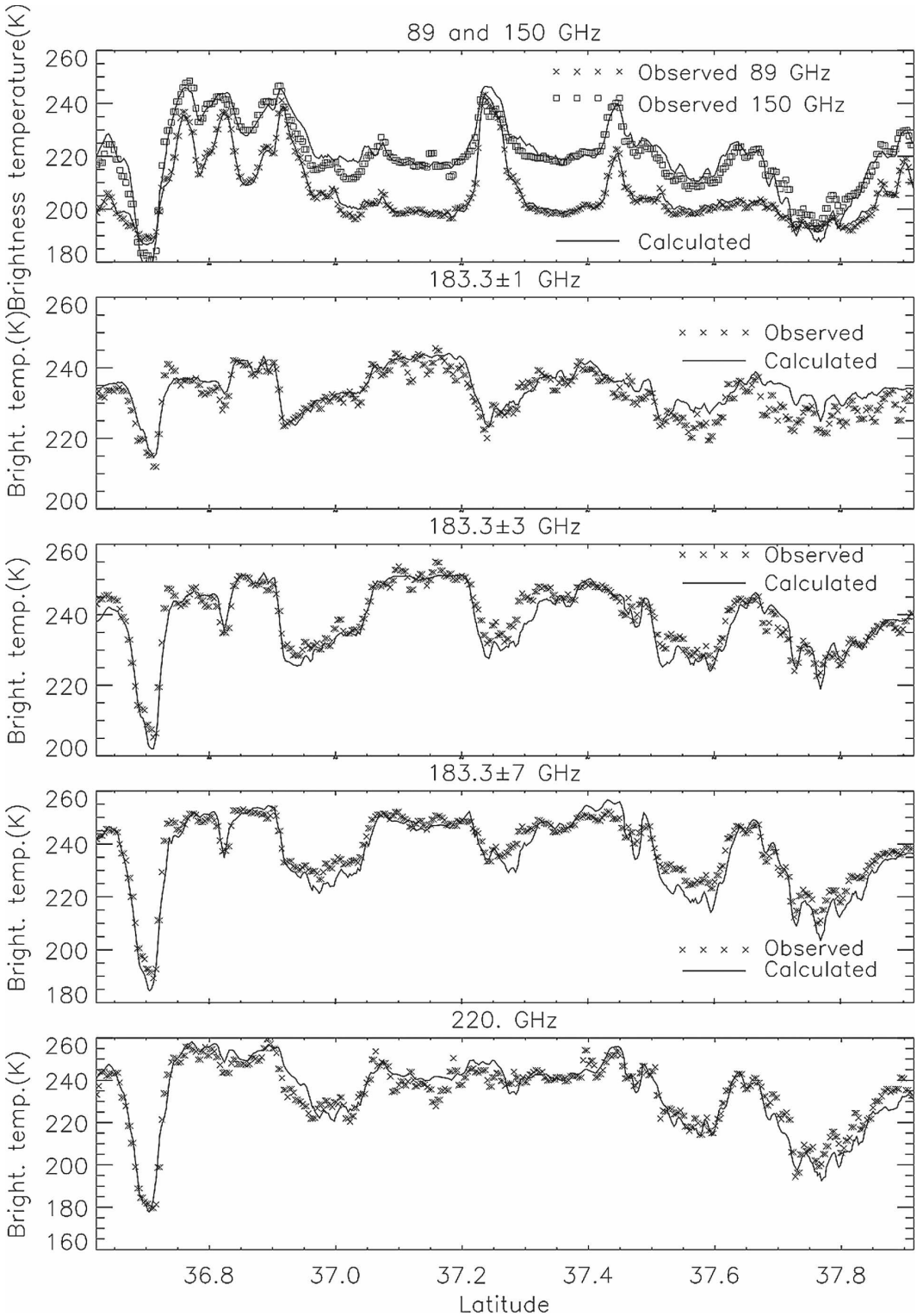

FIG. 6. Observed and simulated brightness temperatures for the 29 Jan 2003 flight leg. The simulated brightness temperatures are derived from the combined cloud radar–millimeter-wave radiometer retrievals.

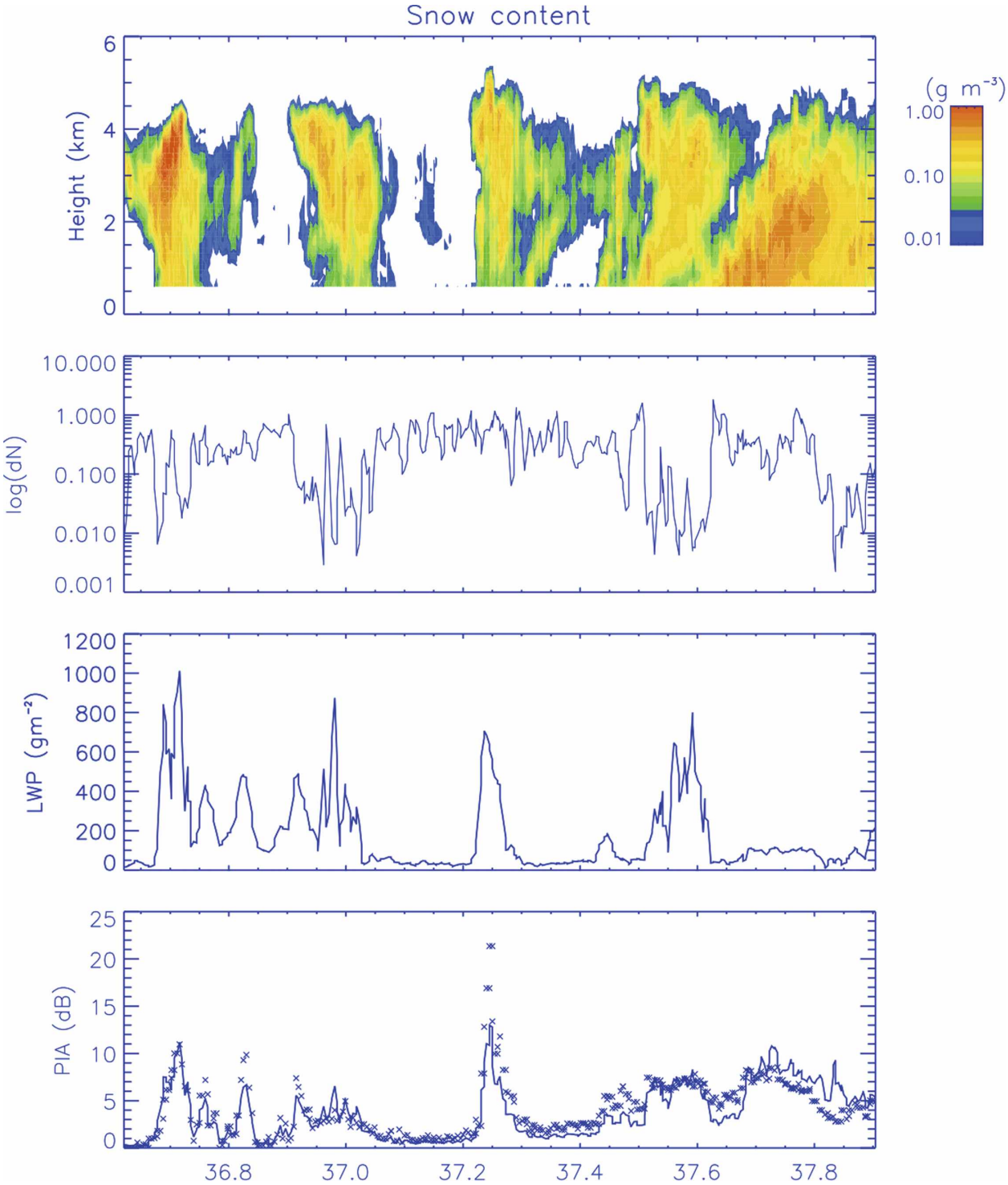

FIG. 7. Retrieved snow content, relative PSD intercept (dN), LWP, and PIA.

the electromagnetic scattering properties is difficult given the limited amount of information in the observations and the ill-posed nature of the retrieval problem. However, the ice water paths of snow from the two retrievals appear to be in reasonably good agreement, although the cause of systematic differences in the vertical structures between the two types of retrievals needs to be further investigated.

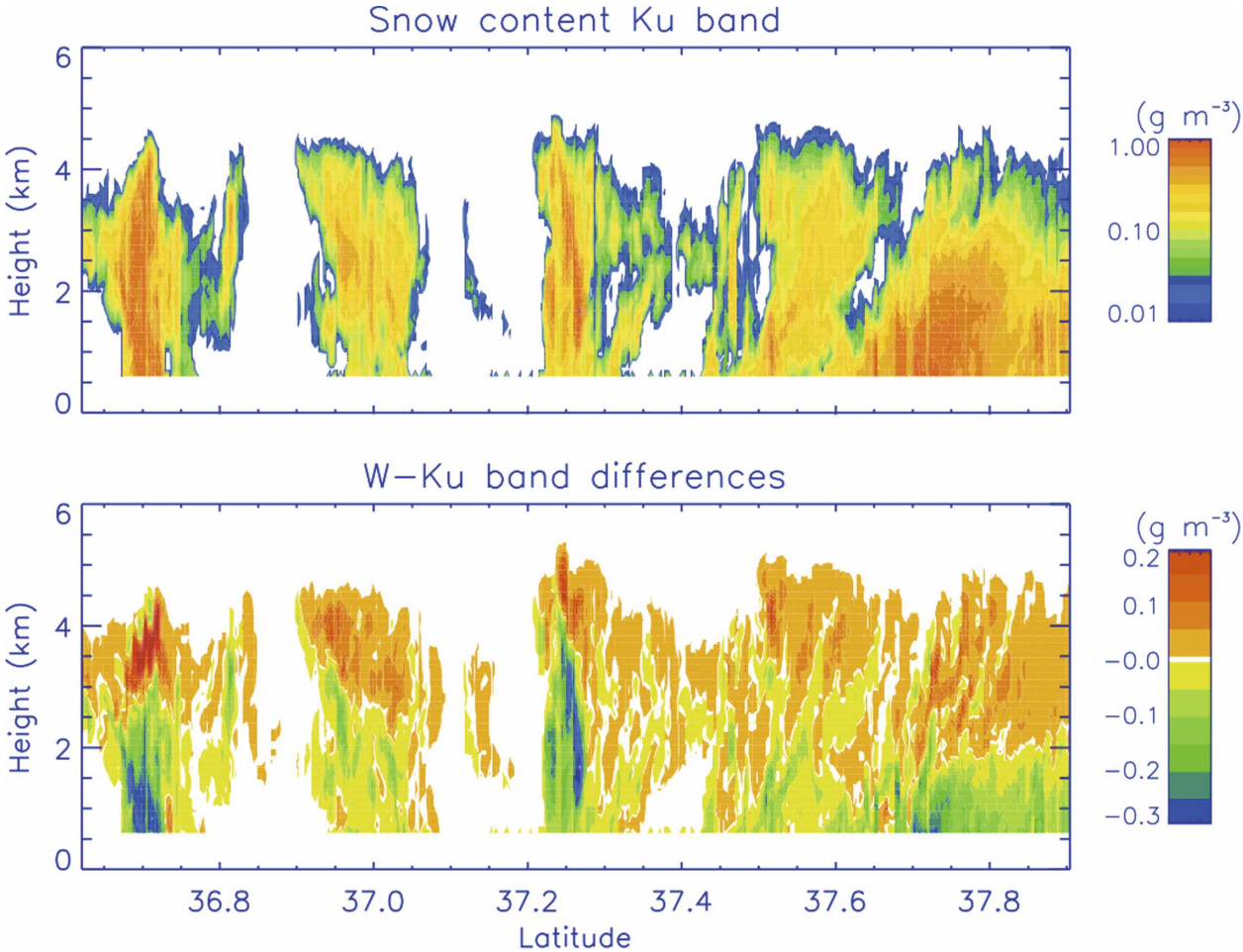

FIG. 8. Retrieved snow from combined Ku-band radar and MIR radiometer observations, and differences between combined W-band–MIR retrievals and Ku-band–MIR retrievals.

To study the combined algorithm's sensitivity to uncertainties in the snow density, the relationship (5) is modified to yield densities that are 2 times as large, and the retrieval algorithm is reapplied to the combined cloud radar and radiometer observations. The agreement between predicted and observed brightness temperatures (not shown) is similar to that illustrated in Fig. 5. However, as noted in the numerical experiment based on synthetic observations, the overall snow content values decrease by about 12.5%. This is an indication that the snow density has to be specified in the algorithm based on independent considerations, that is, using parameterizations derived from microphysical observations and/or simulations employing CRMs with explicit microphysics.

6. Conclusions

In this study, an algorithm to retrieve snow from combined cloud radar and millimeter-wave radiometer observations is developed and investigated. The electromagnetic scattering properties of snowflakes are determined based on calculations using the discrete dipole approximation approach of Draine and Flatau (1994) and the generalized multiparticle Mie approach of Xu and Gustafson (2001). The scattering properties of various ice crystal habits—namely, single cylinders, two orthogonal cylinders, and aggregates of osculating sphere—are calculated using the DDA and GMM approaches. Based on these calculations, electromagnetic scattering properties deemed to be representative of snowflakes in general are determined.

To develop and test the retrieval algorithm, a lake-effect snowstorm is numerically simulated using a CRM. Cloud radar and millimeter-wave radiometer observations are synthesized from the cloud-model output. The retrieval problem is formulated as a minimization problem and is addressed through an iterative Newton method based on the statistical estimation of

the objective function gradient. The application of the retrieval algorithm to the synthetic data yields unbiased results provided that the snow density is correctly parameterized. However, even if the assumed snow density is in error by a factor of 2, only a 15% bias of estimated snow water contents results.

The application of the retrieval algorithm to actual data from the Wakasa Bay field experiment yields snow estimates consistent with both the cloud radar and radiometer observations. Moreover, the estimates are, overall, similar (although systematic differences in the vertical structure are apparent) to estimates from the same algorithm applied to combined Ku-band and millimeter-wave radiometer observations. This is an indication that the attenuation correction, normally provided by radar-derived PIA estimates (but not available at Ku band), can be performed with the addition of millimeter-wave radiometer observations. However, the snow estimates are somewhat sensitive to assumptions made about the snow density, with a 12.5% bias resulting from a factor-of-2 error in the assumed snow density.

Future studies must be conducted to determine the most appropriate snow density parameterizations for algorithm applications. The relationship between the equivalent density and the PSD slope used in this study is believed to apply to dry large snowflakes (Magono and Nakamura 1965), but microphysical data from snowstorms are necessary to confirm whether this relationship is applicable to snowfall retrievals in general.

The algorithm developed in this study is also applicable to satellite data. High-resolution observations from CloudSat cloud-profiling radar are readily available. However, given the low resolution of existing spaceborne millimeter-wave radiometers, such as Advanced Microwave Sounding Unit (AMSU)-B, further studies should be conducted to determine how the radiometer information can improve CPR retrievals. Other radiometers, such as AMSR-E, can also be used to potentially enhance CPR snow estimates. The snow and cloud water distributions derived from airborne observations in this study can be used to simulate CPR and AMSR-E observations realistically, and a retrieval algorithm similar to the one presented here can be developed and tested based upon these synthesized data. The development of an algorithm to retrieve precipitating snow from combined spaceborne radar and radiometer observations would be extremely valuable for the development of accurate radiometer-only method for estimating snow: As shown in Shin and Kummerow (2003), Seo and Liu (2005), Grecu and Olson (2006), and others, accurate, high-resolution precipitation distributions can be used to create a priori datasets of candidate solutions for radiometer-only estimation techniques.

Acknowledgments. This research was supported by the NASA Precipitation Measuring Missions. The authors are grateful to Dr. R. Kakar (NASA Headquarters), Dr. Scott Braun (TRMM Project Scientist), Dr. Arthur Hou (GPM Project Scientist), and Dr. Robert Adler (former TRMM Project Scientist) for their support.

REFERENCES

Cooper, K. A., M. R. Hjelmfelt, R. G. Derickson, D. A. R. Kristovich, and N. F. Laird, 2000: Numerical simulation of transitions in boundary layer convective structures in a lake-effect snow event. *Mon. Wea. Rev.,* **128,** 3283–3295.

Draine, B. T., and P. J. Flatau, 1994: Discrete-dipole approximation for scattering calculations. *J. Opt. Soc. Amer.,* **11A,** 1491.

Evans, K. F., J. R. Wang, P. E. Racette, G. Heymsfield, and L. Li, 2005: Ice cloud retrievals and analysis with the compact scanning submillimeter imaging radiometer and the cloud radar system during CRYSTAL FACE. *J. Appl. Meteor.,* **44,** 839–859.

Evensen, G., 2006: *Data Assimilation: The Ensemble Kalman Filter.* Springer, 280 pp.

Field, P. R., and A. J. Heymsfield, 2003: Aggregation and scaling of ice crystal size distributions. *J. Atmos. Sci.,* **60,** 544–560.

Filippov, A. V., M. Zurita, and D. E. Rosner, 2000: Fractal-like aggregates: Relation between morphology and physical properties. *J. Colloid Interface Sci.,* **229,** 261–273.

Gelb, A., Ed., 1974: *Applied Optimal Estimation.* MIT Press, 374 pp.

Gill, P. E., W. Murray, and M. H. Wright, 1981: *Practical Optimization*. Academic, 401 pp.

Grecu, M., and E. N. Anagnostou, 2002: Use of passive microwave observations in a radar rainfall-profiling algorithm. *J. Appl. Meteor.,* **41,** 702–715.

——, and W. S. Olson, 2006: Bayesian estimation of precipitation from satellite passive microwave observations using combined radar–radiometer retrievals. *J. Appl. Meteor. Climatol.,* **45,** 416–433.

Heymsfield, A. J., and C. M. R. Platt, 1984: A parameterization of the particle size spectrum of ice clouds in terms of the ambient temperature and the ice water content. *J. Atmos. Sci.,* **41,** 846–855.

——, A. Bansemer, P. R. Field, S. L. Durden, J. L. Stith, J. E. Dye, W. Hall, and C. A. Grainger, 2002: Observations and parameterizations of particle size distributions in deep tropical cirrus and stratiform precipitating clouds: Results from in situ observations in TRMM field campaigns. *J. Atmos. Sci.,* **59,** 3457–3491.

Hitschfeld, W., and J. Bordan, 1954: Errors inherent in the radar measurement of rainfall at attenuating wavelengths. *J. Meteor.,* **11,** 58–67.

Iguchi, T., and R. Meneghini, 1994: Intercomparison of single-frequency methods for retrieving a vertical rain profile from airborne or spaceborne radar data. *J. Atmos. Oceanic Technol.,* **11,** 1507–1516.

Kim, M.-J., 2006: Single scattering parameters of randomly ori-

ented snow particles at microwave frequencies. *J. Geophys. Res.,* **111,** D14201, doi:10.1029/2005JD006892.

Kristovich, D. A. R., 1993: Mean circulations of boundary-layer rolls in lake-effect snow storms. *Bound.-Layer Meteor.,* **63,** 293–315.

Kummerow, C., and Coauthors, 2001: The evolution of the Goddard Profiling Algorithm (GPROF) for rainfall estimation from passive microwave sensors. *J. Appl. Meteor.,* **40,** 1801–1820.

Lin, Y.-L., R. D. Farley, and H. D. Orville, 1983: Bulk parameterization of the snow field in a cloud model. *J. Climate Appl. Meteor.,* **22,** 1065–1092.

Lobl, E. S., K. Aonashi, B. Griffith, C. Kummerow, G. Liu, M. Murakami, and T. Wilheit, 2007: Wakasa Bay: An AMSR precipitation validation campaign. *Bull. Amer. Meteor. Soc.,* **88,** 551–558.

Magono, C., and T. Nakamura, 1965: Aerodynamic studies of falling precipitation particles. *J. Meteor. Soc. Japan,* **43,** 139–147.

Maruyama, K., and Y. Fujiyoshi, 2005: Monte Carlo simulation of the formation of snowflakes. *J. Atmos. Sci.,* **62,** 1529–1544.

Marzano, F. S., A. Mugnai, G. Panegrossi, N. Pierdicca, E. A. Smith, and J. Turk, 1999: Bayesian estimation of precipitating cloud parameters from combined measurements of spaceborne microwave radiometer and radar. *IEEE Trans. Geosci. Remote Sens.,* **37,** 596–613.

Meneghini, R., T. Iguchi, T. Kozu, L. Liao, K. Okamoto, J. A. Jones, and J. Kwiatkowski, 2000: Use of the surface reference technique for path attenuation estimates from the TRMM precipitation radar. *J. Appl. Meteor.,* **39,** 2053–2070.

Noh, Y.-J., G. Liu, E.-K. Seo, J. R. Wang, and K. Aonashi, 2006: Development of a snowfall retrieval algorithm at high microwave frequencies. *J. Geophys. Res.,* **111,** D22216, doi:10.1029/2005JD006826.

North, G. R., 1984: Empirical orthogonal functions and normal modes. *J. Atmos. Sci.,* **41,** 879–887.

Olson, W. S., P. Bauer, C. D. Kummerow, Y. Hong, and W.-K. Tao, 2001: A melting-layer model for passive/active microwave remote sensing applications. Part II: Simulation of TRMM observations. *J. Appl. Meteor.,* **40,** 1164–1179.

Seo, E.-K., and G. Liu, 2005: Retrievals of cloud ice water path by combining ground cloud radar and satellite high-frequency microwave measurements near the ARM SGP site. *J. Geophys. Res.,* **110,** D14203, doi:10.1029/2004JD005727.

Shin, D.-B., and C. Kummerow, 2003: Parametric rainfall retrieval algorithms for passive microwave radiometers. *J. Appl. Meteor.,* **42,** 1480–1496.

Skofronick-Jackson, G. M., J. R. Wang, G. M. Heymsfield, R. Hood, W. Manning, R. Meneghini, and J. A. Weinman, 2003: Combined radiometer–radar microphysical profile estimations with emphasis on high-frequency brightness temperature observations. *J. Appl. Meteor.,* **42,** 476–487.

Tao, W.-K., and J. Simpson, 1993: Goddard cumulus ensemble model. Part I: Model description. *Terr. Atmos. Oceanic Sci.,* **4,** 35–72.

Testud, J., S. Oury, R. A. Black, P. Amayenc, and X. Dou, 2001: The concept of "normalized" distribution to describe raindrop spectra: A tool for cloud physics and cloud remote sensing. *J. Appl. Meteor.,* **40,** 1118–1140.

Weinman, J. A., and M.-J. Kim, 2007: A simple model of the millimeter-wave scattering parameters of randomly oriented aggregates of finite cylindrical ice hydrometeors. *J. Atmos. Sci.,* **64,** 634–644.

Westbrook, C. D., R. C. Ball, P. R. Field, A. J. Heymsfield, 2004: Universality in snowflake aggregation. *Geophys. Res. Lett.,* **31,** L15104, doi:10.1029/2004GL020363.

Xu, Y.-L., and B. Å. S. Gustafson, 2001: A generalized multiparticle Mie-solution: Further experimental verification. *J. Quant. Spectrosc. Radiat. Transfer,* **70,** 395–419.

Xue, M., K. K. Droegemeier, and V. Wong, 2000: The Advanced Regional Prediction System (ARPS)—A multi-scale nonhydrostatic atmospheric simulation and prediction model. Part I: Model dynamics and verification. *Meteor. Atmos. Phys.,* **75,** 161–193.